Power Flux and Electric Current Flow to the Divertor Target Plates of JET

J Lingertat, K Günther, A Loarte.

JET Joint Undertaking, Abingdon, Oxon, OX14 3EA.

Abstract

Divertor plate heat loads are recognised as a critical design issue for large power tokamaks. Target heat load data obtained during high power divertor discharges at JET show a large, narrow peak of power flux near the strike point of the separatrix and in the same region an electric current flowing from the target to the plasma. We present an analytical model which connects both phenomena and gives some insight into the underlying physics.

1. Introduction

One of the unresolved key issues in the design of a future fusion reactor is the power handling capability of the divertor target plates. There are numerous technical problems concerning the choice of materials and the design of the power receiving parts. Additionally, the physics behind the transport of particles and energy from the plasma to the target plates is only partly understood. This situation is improving by performing dedicated experiments on high power machines combined with theoretical and modelling efforts to understand the experimental results.

In JET, high power divertor discharges have been performed with a specific emphasis on divertor physics issues. A thorough analysis of the spatial distribution of the target heat load and the currents flowing between the plasma and target shows substantial deviations from the commonly accepted picture of the plasma-target interaction. This paper shows examples of experimental results published in more detail elsewhere [1,2,3] and develops a simple analytical model which gives some insight into the underlying physics.

2. Experimental results

2.1 Power fluxes

Narrow power deposition profiles and electric current flow between the target and the plasma have been observed in various series of well-diagnosed divertor discharges at JET. The results apply mainly to NB-heated single-null discharges with typical parameters I_p = 3.1 MA, B_t = 2.8/3.2 T, $<n_e>$ = 1.7 - 3.8×10^{19} m^{-3}, P_{NB} = 10/15 MW, X-point target distance = 8/13 cm and for both directions of the $\vec{\nabla}B \times \vec{B}$ drift. As a typical example, fig. 1 shows power deposition profiles on the divertor tar-

get plates derived from Langmuir probe data, using the standard formula $q = \gamma \cdot I_{sat} \cdot T_e/e$ with $\gamma = 7$, together with surface temperature profiles obtained by a CCD camera measuring the thermal radiation. The low dynamic range of the CCD camera does not allow a satisfactory conversion of the temperature data into a power flux profile. However, a rough estimate shows that the maximum power flux derived from the temperature data is at least by a factor of 3 higher than that obtained by extrapolating the probe data towards the separatrix. The temperature profile width at the target is extremely small during H-mode (δ_H = 1.5 - 4 cm), during L-mode it is larger (δ_L = 3 - 6 cm). The corresponding power flux profile width should generally be smaller or equal to $\delta_{L,H}$. The flux expansion factor between the outer midplane and the target plate is ≈ 15, so the profile width at midplane becomes during H-mode 1 - 3 mm. The profiles derived from Langmuir probe data are much broader with a decay length of ≈ 7 cm (H-mode) at the target.

Integrating the power flux in the narrow profile over the toroidal length shows that it contributes substantially to the total power dumped on the target [1,3].

The existence of peaked power flux profiles on divertor target plates has recently been confirmed on Asdex-Upgrade with high resolution thermography [4].

2.2 Electric currents

Target probes operated near the strike point of the separatrix show as a rule a high positive current at zero voltage I_0 flowing out of the tile. The same behaviour has been previously reported from DIII-D [5,6]. At JET currents $I_0 \geq 10$ A/cm^2 have been regularly observed for both L and H confinement regimes, both directions of the toroidal field as well as for the inner and outer strike zones.

Fig. 2 shows as an example the profiles of I_0 at the target for a NB heated discharge during the L - and H - mode. Here, the X-point position is constant during both phases and one of the probes is near the outer separatrix. Strong currents ($j_{max} \geq 2 \cdot I_{sat}$) flowing from the plate to the plasma are observed near the strike point superimposed on the well known (and smaller) thermoelectric currents [7, 8, 9] that flow from the outer (hotter) to the inner (colder) strike zone.

Fig. 3 shows the current profile for a different discharge with higher spatial resolution (swept X-point). Clearly, the current flows near both strike points in the same direction which implies the existence of a return current in the outer and inner region of the target plate and the existence of a current flowing perpendicular to the magnetic

field lines somewhere in the SOL. That means the plasma flow towards the target is locally non-ambipolar which is in contradiction to the usual treatment of boundary conditions in most plasma codes.

3. Qualitative physical model

In previous papers [2,3] we speculated that both features, the current flow pattern and the narrow power flux profile, have a common origin. A qualitative discussion of the processes involved starts with the commonly used assumption that the sheath potential Ψ_A follows the electron temperature T_e^* near the target plate ($\Psi_A \approx 3 \cdot T_e^*$). If we assume that the electron temperature decreases with the distance from the strike point this implies that an electric field exists which points away from the separatrix. This field causes an electric current $j_\perp$ to flow perpendicular to the field lines and the plasma to drift in the $\vec{E} \times \vec{B}$ direction. Since this current flows across the magnetic field it experiences a $\vec{j} \times \vec{B}$ force. In steady-state this force has to be compensated by a force $\vec{R}$ of equal magnitude and opposite direction. We assume that $\vec{R}$ is generated by friction of the drifting plasma, and that charge exchange between ions and neutrals is the main source of friction. Continuity of the electric current requires the current to flow in a closed loop. Together with the experimental observations that means: the current has to leave the target near the strike point and to return further outside. Such a current flow out and into the target can only be sustained if the sheath potential relaxes from its ambipolar value. In the region, where the current leaves the target the "non-ambipolar potential" Ψ_N should be smaller than its ambipolar Ψ_A value and where the current flows into the target it should exceed its ambipolar value.

The deviation of the sheath potential from its ambipolar value has an additional effect: The power transmission factor becomes larger than its ambipolar value near the strikepoint and slightly smaller further out, i.e. the power flux profile becomes narrower and steeper.

Although our qualitative discussion describes the experimentally observed phenomena quite well, only a quantitative self-consistent theoretical model can answer the important question about the magnitude of the postulated effects and their relevance for future fusion reactors. Obviously, such a model requires a full 2-D treatment of the SOL using the fluid equations with all relevant drift terms, allowing for current flow in arbitrary directions and using the correct boundary conditions [10]. Here we

try to simplify the problem significantly, aiming at an analytical description of the relevant features.

4. Fluid equations

We adapt a theoretical approach used by one of the authors to derive the characteristics of target mounted Langmuir probes. For details the reader is referred to [11].

The model uses fluid equations in slab geometry, where y is the coordinate along the target plate and x is parallel to the magnetic field lines. Z is an ignorable coordinate ($\partial/\partial z = 0$), the strike point is at y=0 and the magnetic field B is assumed to be constant.

We use the standard fluid equations for continuity (1a,b,c), total momentum balance (2) and electron momentum balance (3).

$$\vec{\nabla} \bullet \vec{j} = 0 \qquad\qquad \vec{\nabla} \bullet \vec{\Gamma} = S \qquad\qquad S = k \cdot N \cdot n \quad , \qquad \text{(1a,b,c)}$$

$$m_i \cdot \vec{\nabla} \bullet \vec{\Gamma}\vec{\upsilon} + \vec{\nabla}p = \vec{j} \times \vec{B} + \vec{S}_m \qquad\qquad \vec{S}_m = -\mu \cdot S \cdot m_i \cdot \vec{\upsilon} \quad , \qquad \text{(2)}$$

$$e \cdot n \cdot \vec{\upsilon} \times \vec{B} = e \cdot n \cdot \vec{\nabla}U - \vec{\nabla}p_e + \vec{j} \times \vec{B} - e \cdot D \cdot \vec{\nabla}n \times \vec{B}, \qquad \text{(3)}$$

where k is the ionisation rate coefficient and μ the ratio of rate coefficients for charge exchange and ionisation assuming cold neutrals. Viscosity and conductivity are neglected ($\eta_{\parallel} = \eta_{\perp} = 0$, $\sigma_{\parallel} = \sigma_{\perp} = 0$) and only the external magnetic field is taken into account. As boundary conditions at the sheath edge we use the Bohm criterion

$$\upsilon(x = \pm L) = \pm c_s^* = \pm \sqrt{(T_e^* + T_i^*)/m_i} \qquad \text{(4)}$$

and from non-ambipolar sheath theory

$$j_x(x = \pm L) = \pm e \cdot n^* \cdot c_s^* \cdot \left\{ 1 - \exp(\Delta - e \cdot U^* / T_e^*) \right\}, \qquad \text{(5)}$$

where Δ is the well-known normalised ambipolar sheath drop

$$\Delta = \ln\left\{ \sqrt{T_e^* / 2 \cdot \pi \cdot m_e} / c_s^* \right\}, \qquad \text{(6)}$$

and the asterisk indicates the sheath edge position (x = ±L).

Considerable simplifications and assumptions are necessary to derive from this set of fluid equations a reasonable and treatable equation for the non-ambipolar potential. Firstly, we assume nearly 100 % replacement of the outstreaming plasma by ionisation, that means

124

$$\vec{\nabla} \bullet \vec{\Gamma} \approx \frac{\partial \Gamma_x}{\partial x} = S, \tag{7}$$

which is usually fulfilled under high recycling conditions.

Secondly, T_e and T_i are assumed to be constant along the field lines and the density has been factorized

$$n = n^*(y) \cdot v(x). \tag{8}$$

Furthermore, we prescribe the profiles of the plasma density, electron temperature and ion temperature to be exponential with different decay lengths λ_n, λ_e, λ_i.

$$n^* = n^*_{e,0} \cdot \exp(-y / \lambda_n) \tag{9}$$

$$T^*_e = T^*_{e,0} \cdot \exp(-y / \lambda_e) \qquad\qquad \zeta(y) = \exp(-y / \lambda_e) \tag{10}$$

$$T^*_i = T^*_{i,0} \cdot \exp(-y / \lambda_i) = T^*_{i,0} \cdot \zeta^{\Lambda_e / \Lambda_i} \qquad \Lambda_{e,i} = \lambda_{e,i} / \lambda_n \tag{11}$$

Here it is important to note that given all these simplifications and assumptions, the results from such a theory will scarcely deliver more than qualitative similarities with the experiment, general trends and some insight into the physical processes.

To derive an equation for the potential we first integrate the longitudinal component of the electron momentum equation along the field lines. The result is an equation for the potential U.

$$U = U^* + \frac{T_e}{e} \cdot \ln(v(x)) \tag{12}$$

In a second step the continuity equation for the electric current is integrated along the field lines. We evaluate the expression $\vec{e}_x \bullet \left[\vec{\nabla} \times \left(\vec{j} \times \vec{B}\right)\right]$ which gives

$$\vec{e}_x \bullet \left[\vec{\nabla} \times \left(\vec{j} \times \vec{B}\right)\right] = B \cdot \frac{\partial j_x}{\partial x}. \tag{13}$$

After integrating (13) over x we obtain

$$-\vec{e}_x \bullet \left[\vec{\nabla} \times \vec{J}\right] = j_x(+L) - j_x(-L) \quad \text{with} \tag{14}$$

$$J = -\frac{1}{B} \int\limits_{-L}^{+L} dx \left\{ m_i \cdot \vec{\Gamma} \bullet \vec{\nabla}\vec{v} + (1 + \mu) \cdot m_i \cdot S \cdot \vec{v} \right\} \tag{15}$$

On the other hand

$$-\vec{e}_x \bullet \left[\vec{\nabla} \times \vec{J} \right] = -\frac{\partial J_z}{\partial y}$$ (16)

The vector $\vec{J}$ in expression (15) has the components $J_y = 0$ and

$$J_z \approx -\frac{2 \cdot m_i \cdot (1+\mu)}{B} \cdot \upsilon_z \cdot n^* \cdot c_s^*.$$ (17)

υ_z in (17) is obtained from (3), (2) and (12)

$$\upsilon_z \approx \frac{1}{B}\left(\frac{dU^*}{dy} + \frac{1}{e}\frac{dT_i}{dy} + \frac{1}{e}\frac{T_i^* \cdot d\ln(n^*)}{dy} \right).$$ (18)

Equating (14) and (16) and inserting (12), (17), (18), (9), (10), (11) gives an ordinary differential equation for the normalised potential $\Psi = e \cdot U^* / T_{e,0}^*$ at the sheath edge

$$\zeta^2 \cdot \frac{d^2\Psi}{d\zeta^2} + \left(\Lambda_e + Q(\zeta) + 1 \right) \cdot \zeta \cdot \frac{d\Psi}{d\zeta} + \left(\Lambda_e + Q(\zeta) + q \right)\left(\Lambda_e + q \right) \cdot \kappa \cdot \zeta^q =$$

$$C\left[1 - \exp(\frac{\Delta \cdot \zeta - \Psi}{\zeta}) \right]$$ (19)

with

$$q = \frac{\lambda_e}{\lambda_i}, \quad Q(\zeta) = \frac{1}{2} \cdot \frac{\zeta + q \cdot \kappa \cdot \zeta^q}{\zeta + \kappa \cdot \zeta^q}, \quad \kappa = \frac{T_i^*}{T_e^*}, \quad C = \frac{\lambda_e^2 \cdot e^2 \cdot B^2}{m_i \cdot T_e^*} \cdot \frac{1}{1+\mu}$$ (20)

The equation is written as a function of the transformed variable ζ (see Eq.10) with the two boundary conditions

$$\Psi'(1) = \frac{d\Psi}{d\zeta}\bigg|_{\zeta=1} = -(\Lambda_e + q)\kappa_0 \quad \text{and} \quad \Psi(0) = 0,$$ (22)

where the first condition means continuity of J_z under the assumption of symmetric profiles in the SOL and in the private flux region and the second vanishing potential at infinity.

Eq. 19 has been solved numerically for a range of the relevant parameters T_e, T_i,

126

λ_e, λ_i and λ_n. The numerical results are used to calculate the current density flowing to the plate j_x and the energy transmission coefficient γ:

$$j_x = j_{\parallel} = e \cdot n^* \cdot c_s^* \cdot \left\{ 1 - \exp(\Delta - e \cdot U^* / T_e^*) \right\},$$

(23)

$$\gamma = 2 \cdot \frac{T_i^*}{T_e^*} + \frac{e \cdot U^*}{T_e^*} + \sqrt{\frac{2 \cdot m_i}{\pi \cdot m_e \cdot (1 + T_i^* / T_e^*)}} \cdot \exp(-\frac{e \cdot U^*}{T_e^*}).$$

(24)

5. Results

Fig. 4 shows as an example one of the profiles obtained. It is obvious that the calculated profiles correspond to the expected ones. For the parameter set chosen in fig. 4 there is a significant difference between the ambipolar and the non-ambipolar potential at the strike point (~ 1.5 $T_{e,0}^*$) which causes a maximum current of ~ 3 I_{sat} to flow from the target plate to the plasma. The width of the current flow channel near the separatrix is rather narrow (~ 0.1 λ_e), whereas the return current is distributed over a much larger area. The energy transmission coefficient has a high maximum near the strikepoint. However, this maximum is caused mainly by the assumed profile of the ion temperature. An additional steepening of the power flux profile results from the current flowing near the separatrix.

Figs. 5 and 6 show the current density at the strike point and the width of the current flow channel near the separatrix as a function of T_i and $\Lambda_i = \lambda_i/\lambda_n$, whilst T_e, λ_e and $\Lambda_e = \lambda_e/\lambda_n$ are held constant at experimentally determined values. From the experiment we know j_{max}/I_{sat} to be ~ 2. Using our model (fig.5), this value can be obtained e.g. for $T_i \sim 200$ eV and $\Lambda_i \sim 0.1$ or $T_i \sim 700$ eV and $\Lambda_i \sim 1$. However, the relevance of these rather high ion temperatures and small decay lengths can only be assessed experimentally or by a 2D-code which avoids the simplifications made in this paper.

The current density increases with increasing T_i and decreasing Λ_i, whereas the width of the current flow channel shows just the opposite behaviour. An analysis of the dependencies on other relevant model parameters reveals that the calculated quantities are most sensitive to the ratios T_i/T_e and λ_i/λ_e. Clearly, this is the result of Eq. (18). In our model the friction force, and hence the maximum current which

can be sustained, depends on the drift velocity. This in turn depends according to (18) on the gradients of the potential and ion pressure.

The calculated profiles describe the experimentally observed well. However, as previously stated, due to the used simplifications and approximations further conclusions should only be drawn after comparison with 2D-code results. It is of particular importance to verify that the high ion temperatures and short decay lengths obtained within the model are consistent with the code predictions.

6. Summary and conclusions

Power flux profiles at the divertor target plates of JET during NB heated X-point discharges show a large, narrow peak near the separatrix overlaid on a smaller and broader exponential tail.

In the region of the narrow power flux peak a large electron current is flowing from the plasma to the target which has the same direction on both target plates. This implies a current flow perpendicular to the magnetic field lines elsewhere in the SOL. An analytical model using non-ambipolar fluid theory has been developed which shows that both phenomena are caused by a common mechanism.

The model qualitatively reproduces the experimental findings. Within the framework of the model the main cause of the observed current flow are the radial gradients of electron temperature and ion pressure.

The current and the energy transmission coefficient at the separatrix increase mainly with increasing T_i/T_e and decreasing λ_i/λ_e, whilst at the same time the widths of the current and power flux profile decrease. Large values for the ratio T_i/T_e or small values for the ratio λ_i/λ_e are required to fit the experimental data.

Further experimental and theoretical research is needed to determine the relevance of the phenomenon to ITER. Especially, results from 2-D fluid codes which include all relevant terms and boundary conditions should give further insight into the physics and allow more reliable extrapolations to high power divertor tokamaks.

7. References

[1]   Lingertat, J. et al.,The behaviour of the divertor target plates during high performance hot-ion mode discharges at JET, JET Report JET-IR(92)09, (1992).

[2]   Loarte, A. et al., Plasma parameters in the vicinity of the separatrix strike points on the divertor target plates in JET, JET Report JET-IR(92)09, (1992).

[3]   Lingertat, J. et al., Poster at the 4th Intern. Workshop on Plasma Edge Theory, Varenna 1993

[4] Herrmann, A., et al., this conference.

[5] Buchenauer, D., et al., Jour. Nucl. Mat. 176&177 (1990) 528.

[6] Schaffer, M.J., et al., Nucl. Fusion 31 (1991) 1750.

[7] Harbour, P.J., et al., Jour. Nucl. Mat. 162 & 164 (1989) 236.

[8] Staebler, G.M., et al., Nucl. Fusion 29 (1989) 1820.

[9] Chankin, A.V., et al., Jour. Nucl. Mat. 196-198 (1992) 739.

[10] Baelmans, M., et al., this conference

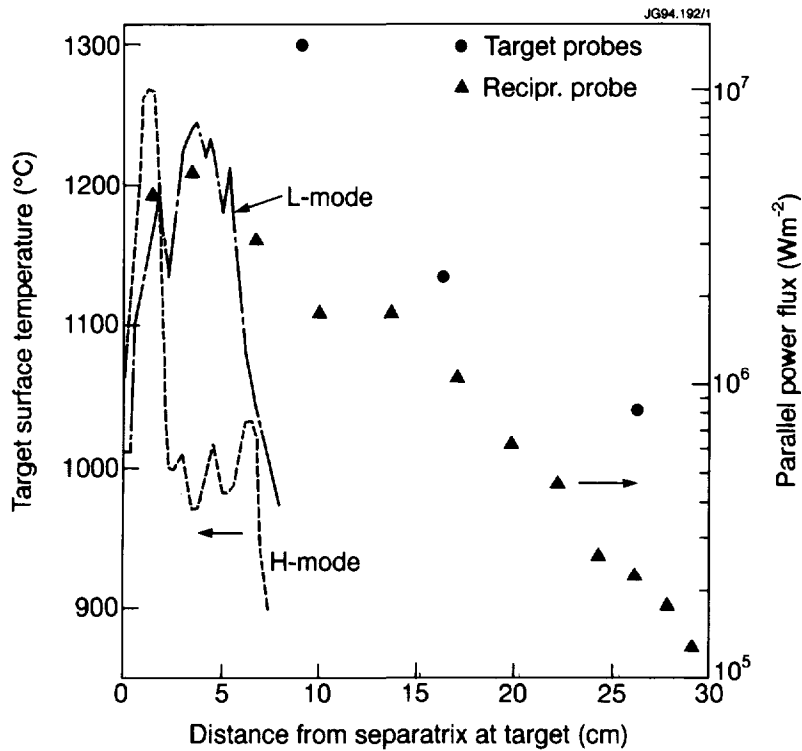[11] Günther, K. et al., Contr. Plasma Physics 34 (1994) 484.

Fig.1 Profiles of the parallel power flux at the divertor target plate derived from Langmuir probes during H-mode and temperature profiles during L- and H-mode from the CCD camera, pulse 25724, outer strike zone.
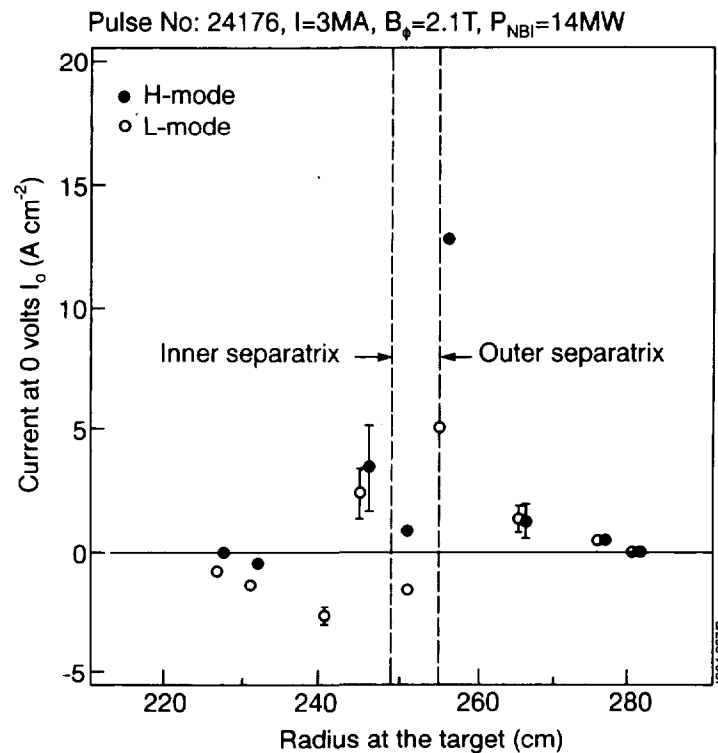

Pulse No: 24176, I=3MA, B_ϕ=2.1T, P_{NBI}=14MW

Fig.2 Current profiles from target mounted Langmuir probes (target on vessel potential) in a pulse with stationary separatrix position (I_0 >0 positive current towards the target).

Pulse No: 26019, I=3MA, B_ϕ=2.9T, P_{NBI}=15.5MW

Inner separatrix   Outer separatrix

I_o (A cm^{-2})

12

8

4

0

-4

SOL

Private flux region

Private flux region

SOL

236 238 240 242 244 246 248 250 252 254
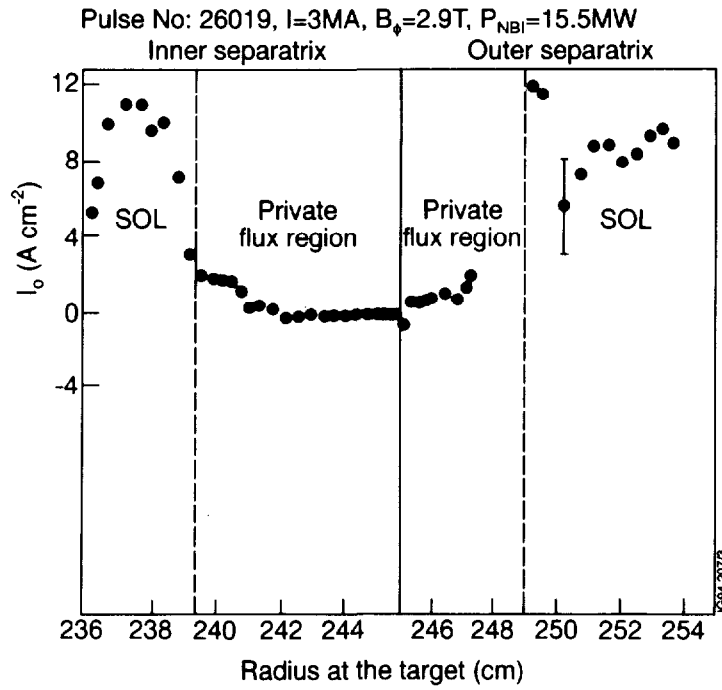
Radius at the target (cm)

JG94.207/3

Fig.3   Current profiles from target mounted Langmuir probes (target on vessel potential) in a pulse with swept separatrix position (I_0 >0   positive current towards the target).
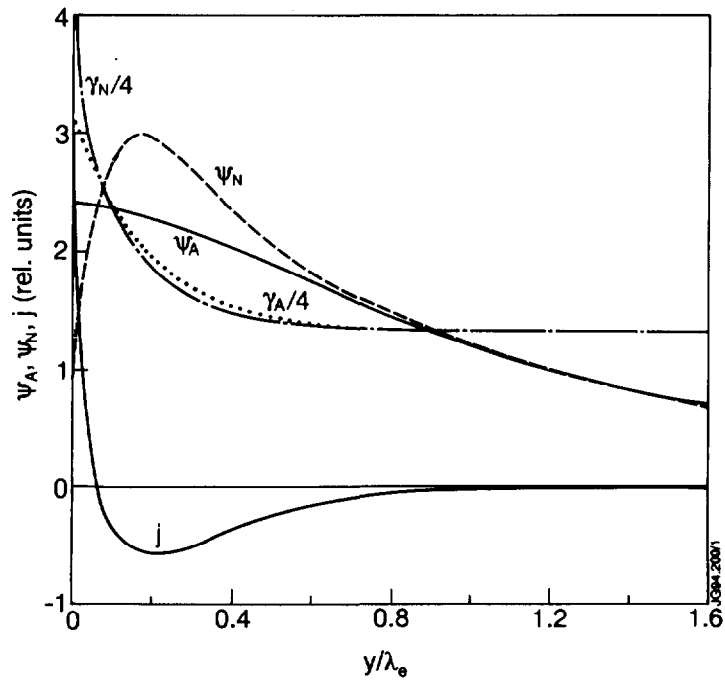
Ψ_A, Ψ_N, j (rel. units)

4

3

2

1

0

-1

0   0.4   0.8   1.2   1.6

$\gamma_N/4$

Ψ_N

Ψ_A

$\gamma_A/4$

j

JG94.200/1

y/λ_e

Fig.4   Calculated profiles of the non-ambipolar potential Ψ_N in units of $T_{e,0}^*$, the current density j in units of I_{sat} and the energy transmission coefficient $\gamma_N/4$ together with the ambipolar profiles Ψ_A and $\gamma_A/4$ (T_i= 400 eV, Λ_i = 0.5, T_e = 100 eV, λ_e =1 cm, Λ_e =3, B = 3 T, A = 2, μ = 2)
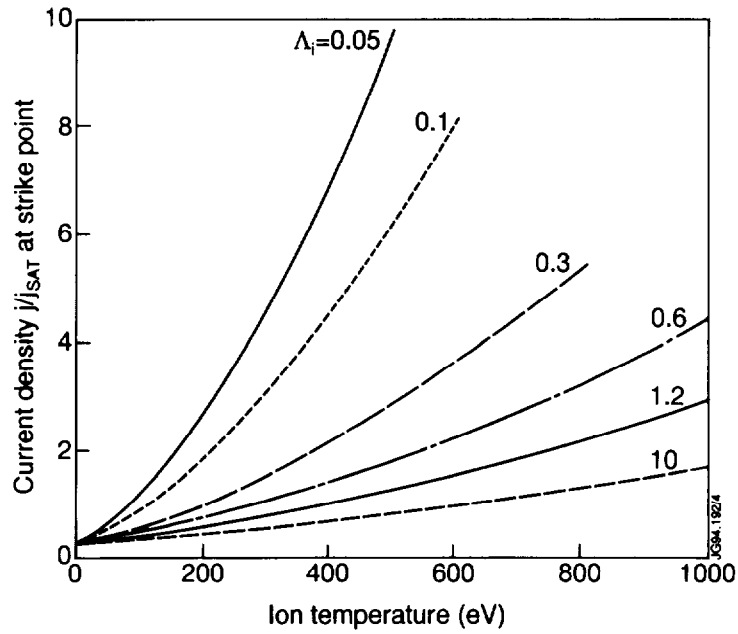
131

Fig.5 Calculated current density at the strike point as a function of ion temperature for different parameters Λ_i (T_e = 100 eV, λ_e =1 cm, Λ_e =3, B = 3 T, A = 2, μ = 2).
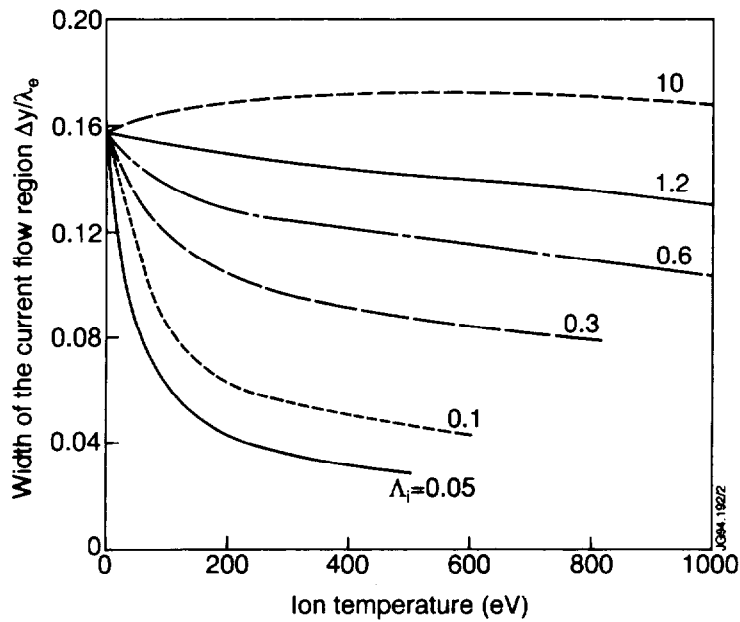

Fig.6 Calculated width of the current flow region near the separatrix as a function of ion temperature for different parameters Λ_i (T_e = 100 eV, λ_e =1 cm, Λ_e =3, B = 3 T, A = 2, μ = 2).